Highlights

Effective medium modelling of real-world multi-modal metamaterial panels achieving broadband vibroacoustic attenuation

Daniele Giannini, Edwin P.B. Reynders

- Multi-modal metamaterials exploit multiple translational and rotational resonator modes for broadband effectiveness.
- An effective medium model for real-world multi-modal metamaterial panels is developed.
- The approach handles arbitrary finite sizes, boundary conditions, and resonator distributions.
- Combination with Det-SEA allows for efficient diffuse STL predictions.
- The proposed effective medium modelling approach is validated against detailed FEM.

Postprint submitted to Extreme Mechanics Letters

Published version: D. Giannini and E.P.B. Reynders. Effective medium modelling of real-world multi-modal metamaterial panels achieving broadband vibroacoustic attenuation. Extreme Mechanics Letters, 69:102161, 2024. https://doi.org/10.1016/j.eml.2024.102161

Effective medium modelling of real-world multi-modal metamaterial panels achieving broadband vibroacoustic attenuation

Daniele Giannini[a], Edwin P.B. Reynders[a]

[a]*Department of Civil Engineering - Structural Mechanics Section, KU Leuven, Kasteelpark Arenberg 40 Leuven, 3001, Belgium*

Abstract

Locally resonant metamaterials can achieve unprecedented vibroacoustic performance by subwavelength distributions of small mechanical resonators on a host structure. Substantial broadband vibroacoustic attenuation can be achieved by multi-modal metamaterial panels, which exploit multiple translational and rotational resonator modes to manipulate the overall bending wave propagation. However, the multi-modal metamaterial concept has been studied only for idealized conditions, such as infinite panel extent and uniformly distributed resonators, limiting practical applicability. Efficient methodologies are still needed to study the behaviour of multi-modal metamaterial panels in real-world scenarios. In this work, this challenge is tackled by developing generalized effective medium models, i.e., homogenized material representations through equivalent macro-scale properties, tailored for finite-sized multi-modal metamaterial panels. For the special but important case of simply supported rectangular panels with uniformly distributed resonators, a dedicated analytical effective medium model is developed. For arbitrary boundary conditions and resonator distributions, effective medium finite elements are formulated. The diffuse sound transmission loss (STL) performance is efficiently predicted through Deterministic - Statistical Energy Analysis (Det-SEA), by coupling the effective medium model of the finite-sized metamaterial panel with a diffuse model of the surrounding sound fields. The proposed prediction approaches are validated against detailed FEM modelling, demonstrating that significant computational reductions are achieved while preserving accuracy. Results showcase that multi-modal metamaterial panels maintain broadband vibracoustic attenuation also when subjected to boundary effects and under partial metamaterial treatment.

Keywords: multi-modal metamaterial panels, effective medium model, vibroacoustic attenuation, sound insulation, finite-size effects, deterministic-statistical energy analysis

1. Introduction

Locally resonant metamaterials are a revolutionary technology to achieve unprecedented vibroacoustic properties that are not naturally found in conventional materials [1, 2, 3]. Metamaterials can lead to outstanding vibration attenuation and sound insulation performance in partition panels [4, 5, 6, 7], with a high potential impact in multiple domains, including mechanical, civil, marine, automotive, and aerospace engineering. These exceptional properties are achieved by creating bandgaps for plate bending waves, i.e. frequency ranges in which bending wave propagation is stopped, through the addition of small mechanical resonators on a subwavelength scale [8, 9, 10, 11].

While traditional metamaterial panels employ predominantly single-mode translational resonators, different strategies have emerged to extend the frequency band of effectiveness. Multiple resonators can be combined in series [12, 13, 14] or in parallel [4, 15, 16]. Locally resonant bandgaps can be combined with Bragg scattering effects [17]. The synergy of mechanical and acoustic resonances can be exploited [18]. The resonator design can be progressively varied within the host structure domain, achieving graded metamaterials [19]. Furthermore, the use of multi-modal metamaterial panels has been recently proposed. Here multiple translational and rotational modes are combined within a single resonator to achieve broadband effectiveness [20]. However, the multi-modal metamaterial concept has been studied only for idealized conditions, such as infinite panel extent and uniformly distributed resonators. Efficient methodologies are still needed to study the behaviour of multi-modal metamaterial panels in real-world scenarios, i.e. in the presence of finite-size effects, arbitrary boundary conditions, and non-uniform resonator distributions.

The vibroacoustic properties of metamaterial panels can be numerically predicted through periodic unit cell modelling. In this case, one single, periodically repeated, unit cell is modelled in detail, e.g., with the finite element (FE) method, and periodicity conditions are imposed at its boundaries. When assuming infinite panel extent, the created bandgaps and the achieved sound transmission loss (STL) can be studied e.g. through a wave and finite

element method [21]. Finite-size effects can be approximated e.g. through the hybrid analytical-numerical approach proposed in [22]. In this case, the impedance of the panel is numerically computed through unit cell modelling, the radiation impedance is derived when accounting for the finite area of the panel, and analytical expressions are used to predict sound insulation. To additionally consider the modal behaviour of the finite panel, the unit cell periodicity conditions can be modified so that they comply with the applied boundary conditions [23, 24]. Furthermore, when considering diffuse sound fields surrounding a finite panel, the hybrid deterministic-statistical energy analysis (Det-SEA) framework can be employed to compute the diffuse STL [25]. In this case, a detailed model of the (periodic) finite panel is combined with a diffuse model of the surrounding sound fields [26, 27, 28].

Despite the advantages offered by periodic unit cell modelling, the size of the unit cell FE models can become significant when incorporating resonators with complex geometries, leading to high computational costs. A possible strategy to accelerate calculations is to use reduced order unit cell modelling, e.g. Craig-Bampton reduction or generalized Bloch mode synthesis [29]. However, the general lack of efficient modelling strategies still remains a challenge when designing realizable multi-modal metamaterial panels. Furthermore, unit cell modelling implicitly assumes periodicity and is generally not suitable for modelling non-uniform resonator distributions.

Effective medium models are an appealing alternative to unit cell modelling to further increase computational efficiency [30]. In this case, the metamaterial is studied as a homogenized medium, with effective properties that capture the macro-scale behaviour arising from the micro-scale unit cell structure. Effective medium models have been developed for a broad range of metamaterials involving different physical phenomena, e.g., effective stiffness tensor models for periodic lattice structures [31, 32], effective permittivity and permeability models for electromagnetic metamaterials [33, 34], effective refractive index models for optical metamaterials [35, 36], and effective mass density and bulk modulus models for acoustic metamaterials [37, 38]. Effective mass density models are used also for metamaterial panels with local mechanical resonances, typically for single-mode translational resonators [4, 30, 39, 40]. Recently, techniques have been developed to homogenize both translational and rotational resonator components, enabling the efficient analysis of wave propagation and sound insulation in multi-modal metamaterial panels [20]. However, available effective medium models for metamaterial panels are still based on the assumption of infinite panel dimensions.

This work aims to develop a generalized effective medium modelling framework to study the behaviour of multi-modal metamaterial panels in real-world scenarios. This is achieved by developing appropriate effective medium models for finite-sized metamaterial panels and coupling them with STL predictions based on Det-SEA. For the special but important case of simply supported rectangular metamaterial panels with uniformly distributed resonators, a dedicated analytical effective medium model is first developed by exploiting the sinusoidal mode shapes of the bare plate. To accommodate general boundary conditions and non-uniform distributions of the resonators, e.g. partial metamaterial treatments, effective medium plate finite elements are then developed.

The present manuscript is organized as follows. Section 2 summarizes the features of the existing effective medium modelling framework for infinite-sized multi-modal metamaterial panels. In Section 3, the framework is generalized and coupled with Det-SEA to enable diffuse STL predictions in real-world scenarios. In Section 4, the vibroacoustic properties of multi-modal metamaterial panels are studied when varying the panel dimensions, the applied boundary conditions, and the treatment area. Furthermore, the presented effective medium methodologies are validated against the use of conventional detailed finite element models. Finally, conclusions and remarks are presented in Section 5.

2. Effective medium modelling of multi-modal metamaterial panels with infinite size

This Section summarizes the existing effective medium modelling framework for multi-modal metamaterial panels. It does not contain new developments, but rather introduces fundamental concepts and notations upon which the other Sections are built. The analytical homogenization of translational and rotational resonator components is first discussed, along with their effect on bending wave dispersion and diffuse STL for metamaterial panels with infinite extent. The methodology to include complex multi-modal resonators is then presented.

2.1. Homogenization of translational and rotational resonator components

Referring to Figure 1, the considered metamaterial panel consists of a host Kirchhoff plate, subjected to bending motions, to which resonators are

attached. The translational and rotational resonator components are represented by single-degree-of-freedom systems. The bending deformation of the host plate is described in terms of the transversal displacement $w(x, y, t)$ of its neutral plane. For subwavelength distributions, the mechanical behaviour of the resonators is described by their distributed transversal displacement $u(x, y, t)$ and rotation $\theta(x, y, t)$.

The proposed analytical homogenization procedure assumes time-harmonic motion, for which the degrees of freedom of the resonators are condensed out [20], and the equations of motion of the metamaterial panel are expressed solely in terms of the transversal plate displacement $w(x, y, t) = \overline{w}(x, y)e^{i\omega t}$:

$$\left(D_{\mathrm{x}}\frac{\partial^4\overline{w}}{\partial x^4} + 2H\frac{\partial^4\overline{w}}{\partial x^2\partial y^2} + D_{\mathrm{y}}\frac{\partial^4\overline{w}}{\partial y^4}\right)(1+\mathrm{i}\eta_0) \\ -\omega^2\left[\left(\rho h + a_{\mathrm{z}}(\omega)\right)\overline{w} - a_{\mathrm{rx}}(\omega)\frac{\partial^2\overline{w}}{\partial y^2} - a_{\mathrm{ry}}(\omega)\frac{\partial^2\overline{w}}{\partial x^2}\right] = p \quad (1)$$

where rotational components around both the x- and the y-axis have been considered and:

$$a_{\mathrm{z}}(\omega) = \frac{m''_{\mathrm{z}}(1+\mathrm{i}\eta)}{(1+\mathrm{i}\eta) - (\omega/\omega_{\mathrm{z}})^2}, \qquad a_{\mathrm{rx/ry}}(\omega) = \frac{J''_{\mathrm{rx/ry}}(1+\mathrm{i}\eta)}{(1+\mathrm{i}\eta) + (\omega/\omega_{\mathrm{rx/ry}})^2} \quad (2)$$

Eq. (1) considers an orthotropic host plate: D_{x} and D_{y} are the bending stiffnesses along the directions x and y respectively, H is the torsional stiffness, ρ and h are the mass density and thickness, and η_0 is the damping loss

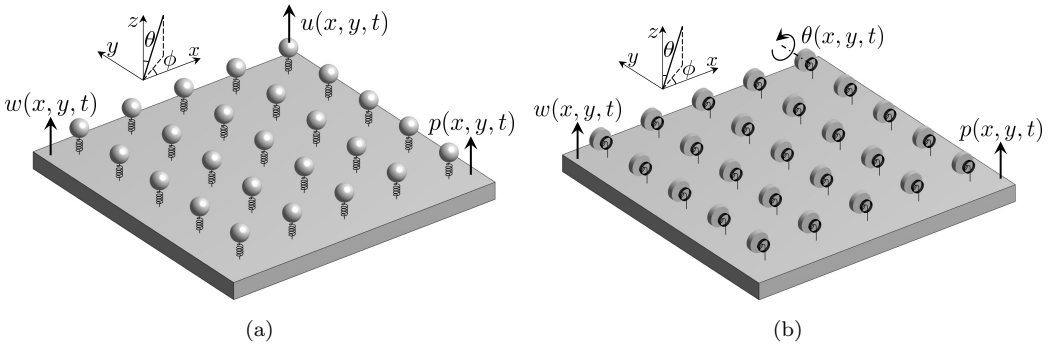


Figure 1: Scheme of (a) translation and (b) rotational components of distributed resonators in metamaterial panels.

factor. The resonators are characterized by the translational and rotational distributed inertia per unit of area m''_{z} and $J''_{\mathrm{rx/ry}}$, the fixed-base natural frequencies ω_{z} and $\omega_{\mathrm{rx/ry}}$, and the damping loss factor η.

By considering a plane wave solution $\overline{w}(x,y) = We^{\mathrm{i}(k_{\mathrm{x}}x+k_{\mathrm{y}}y)}$, Eq. (1) can be reduced to the standard plate bending equation if the plate density is replaced by an effective mass density, which is given by the first expression below when translational resonators are present, and the second one when rotational resonators are present [20]:

$$\rho_{\mathrm{eff,z}} = \rho + \frac{a_{\mathrm{z}}(\omega)}{h}, \qquad \rho_{\mathrm{eff,rx/ry}} = \rho + \frac{a_{\mathrm{rx/ry}}(\omega)k^2_{\mathrm{y/x}}}{h} \tag{3}$$

Eq. (3) shows that the effective mass density associated with the translational resonator components depends only on the frequency of analysis. The contribution of rotational resonator components to the effective mass density is instead scaled by the square of the wavenumber components k_{x} and k_{y} propagating in the panel, indicating that rotational components are more effective at higher wavenumbers and therefore at higher frequencies.

2.2. Effect of the resonator components on bending wave dispersion

The presented effective medium model is used to efficiently predict the dispersion of bending waves in metamaterial panels along a given propagation direction defined by the azimuthal angle ϕ (cf. Figure 1). The dispersion in undamped metamaterial panels ($\eta = \eta_0 = 0$) is expressed through the effective mass density by the following equation:

$$\rho_{\mathrm{eff}}(\omega, k, \phi)h\omega^2 = D(\phi)k(\omega,\phi)^4 \tag{4}$$

which is solved e.g. by imposing the wavenumber $k(\omega,\phi)$ and solving for the frequency ω. In Eq. (4), $D(\phi) = D_{\mathrm{x}}\cos^4\phi + 2H\cos^2\phi\sin^2\phi + D_{\mathrm{y}}\sin^4\phi$ is the bending stiffness of the panel along the direction ϕ.

Two examples of dispersion in metamaterial panels, considering respectively distributed translational resonators and distributed rotational resonators around the y-axis, are shown in Figures 2a and 2b. An orthotropic host panel with the following properties is considered: $h = 0.015$ m, $\rho = 1200$ kg/m^3, $D_{\mathrm{x}} = 1500$ Nm, $D_{\mathrm{y}} = 4500$ Nm, $H = 2598$ Nm, $\eta_0 = 0.05$, which can represent an orthotropically stiffened plate in polymethyl methacrylate (PMMA) [20]. The considered inertial properties of the resonators are $m''_{\mathrm{z}} = \gamma\rho h$, $J''_{\mathrm{ry}} = 3\cdot 10^{-3}$ kg, where the mass ratio $\gamma = 0.1$ expresses the

relative amount of mass added to the host structure by the resonators. Also, the resonance frequencies of the resonators are $f_{\mathrm{z}} = \omega_{\mathrm{z}}/2\pi = f_{\mathrm{ry}} = \omega_{\mathrm{ry}}/2\pi = 1589.5$ Hz. The dispersion curves are computed along the irreducible Brillouin contour of a unit cell with dimensions $L_{\mathrm{x}} \times L_{\mathrm{y}} = 0.05$ m $\times$ 0.05 m. As shown in Figure 2, for attached translational resonators an omnidirectional bandgap is created in the range $\omega_{\mathrm{z}} \leq \omega \leq \omega_{\mathrm{z}}\sqrt{1+\gamma}$, where the effective mass density assumes negative values [40, 20]. For attached rotational resonators, a zero-width directional bandgap is created at ω_{ry} for propagation directions perpendicular to the rotation axis of the resonator, following the directionality of the transferred inertial bending moments to the host plate. This type of directional bandgaps has been also experimentally observed [41].

2.3. Effect of the resonator components on the diffuse STL of metamaterial panels with infinite dimensions

The diffuse STL R of an infinite metamaterial panel is computed by integrating the plane wave transmission coefficient $\tau(\omega, \phi, \theta)$ over all possible incident directions, defined by the azimuthal angle ϕ and the elevation angle θ (cf. Figure 1) [42]:

$$\begin{aligned} R(\omega) &= -10 \log_{10} \tau_{\mathrm{d}} \\ \tau_{\mathrm{d}}(\omega) &= \frac{\int_0^{2\pi} \int_0^{\pi/2} \tau(\phi, \theta) \sin\theta \cos\theta \mathrm{d}\theta \mathrm{d}\phi}{\int_0^{2\pi} \int_0^{\pi/2} \sin\theta \cos\theta \mathrm{d}\theta \mathrm{d}\phi} \end{aligned} \tag{5}$$

For each plane incident sound wave, a bending wave in the panel is induced with trace wavenumber $k = \frac{\omega}{c} \sin\theta$, and projections along the x and y directions $k_{\mathrm{x}} = k\cos\phi$ and $k_{\mathrm{y}} = k\sin\phi$. The effective medium model enables analytically computing the plane wave transmission coefficient as [20]:

$$\tau(\omega, \phi, \theta) = \left| \frac{2\rho_0 c/\cos\theta}{2\rho_0 c/\cos\theta - (\mathrm{j}/\omega)(D(\phi)k^4 - \rho_{\mathrm{eff}} h \omega^2)} \right|^2 \tag{6}$$

where $c = 341$ m/s and $\rho_0 = 1.21$ kg/m^3 are the speed of sound and the mass density in the surrounding air.

The diffuse STL of metamaterial panels with respectively distributed translational and rotational resonators is shown in Figures 2c and 2d, along with the diffuse STL of the bare host plate. Damping loss factors $\eta = \eta_0 = 0.05$ have been considered. The STL curve of the bare host plate shows a broadband dip due to coincidence in the range 1250-2000 Hz, within which

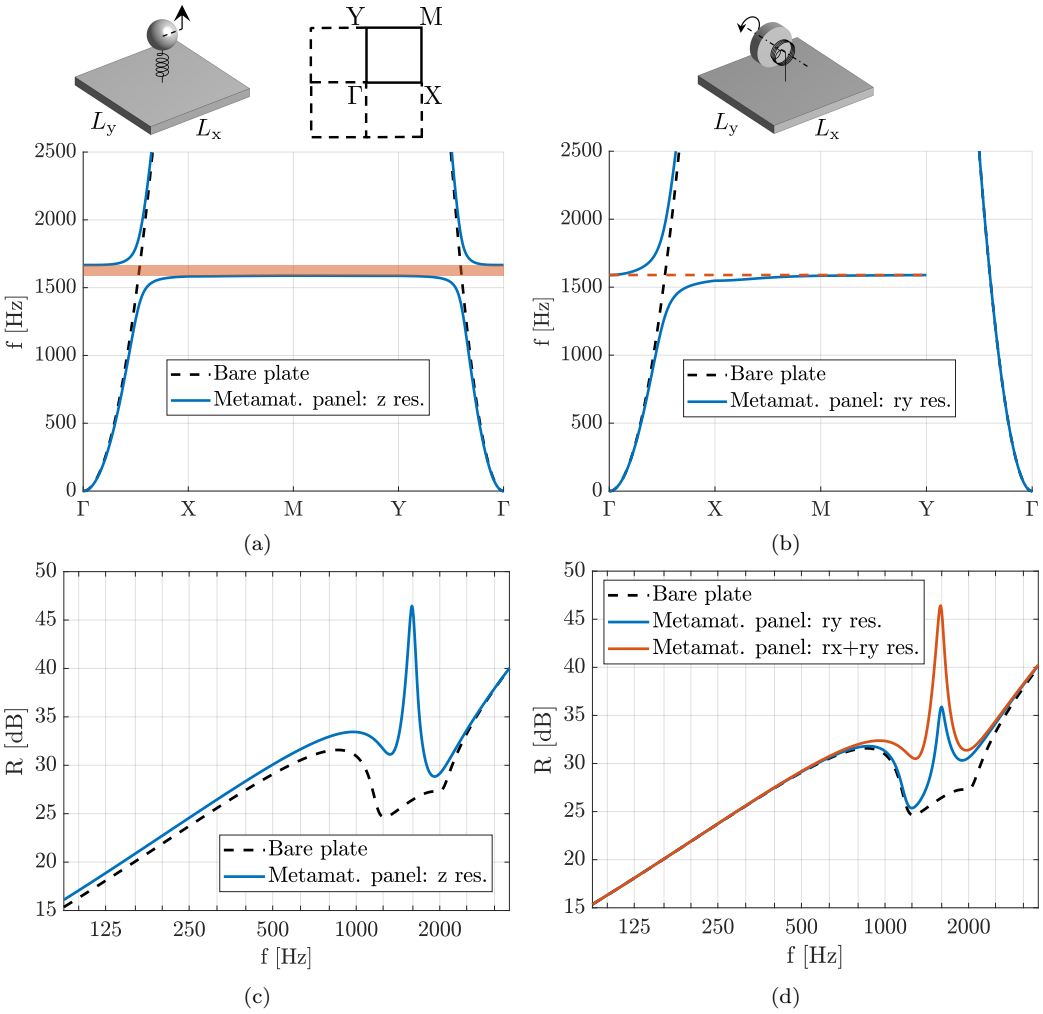


Figure 2: Effect of (a,c) translational and (b,d) rotational resonator components on (a,b) the bending wave dispersion and (c,d) the diffuse STL of metamaterial panels.

the speed of the forced bending waves in the plate can match the speed of the free bending waves along the different orthotropic directions [20]. The STL curves of the metamaterial panels show that both translational and rotational resonator components introduce a STL peak at the corresponding resonance frequency. If this resonance STL peak is within the coincidence dip, a net STL improvement is obtained. A single rotational component around the y-axis can influence only bending wave components propagating along the x-axis, and therefore provides generally smaller STL improvements than translational components. Combining rotational resonator components around the x- and the y- axis influences instead all bending wave components propagating in the panel, and for the proposed examples provides similar improvements to translational components.

2.4. Metamaterial panels with complex multi-modal resonator layouts

Metamaterial panels with complex multi-modal resonator layouts can be studied by combining the translational and rotational inertial contributions of each resonator mode k. These modal inertial contributions are expressed in terms of the modal effective translational and rotational masses $m_{\mathrm{z},k}$ and $J_{\mathrm{rx/ry},k}$, which can be extracted from a single modal analysis of the fixed-base resonator, e.g. after finite element discretization [20]. The effective mass density of the multi-modal metamaterial panel is then obtained as:

$$\rho_{\mathrm{eff}}(\omega, k_{\mathrm{x}}, k_{\mathrm{y}}) = \rho\alpha_{\mathrm{st}} + \frac{1}{h}\sum_{k=1}^{n_{\mathrm{m}}} \left(a_{\mathrm{z},k}(\omega) + a_{\mathrm{rx},k}(\omega)k_{\mathrm{y}}^2 + a_{\mathrm{ry},k}(\omega)k_{\mathrm{x}}^2\right) \tag{7}$$

with:

$$\begin{aligned} \alpha_{\mathrm{st}} &= 1 + \gamma - \sum_{k=1}^{n_{\mathrm{m}}} \frac{m''_{\mathrm{z},k}}{\rho h} \\ a_{\mathrm{z},k}(\omega) &= \frac{m''_{\mathrm{z},k}(1+\mathrm{i}\eta)}{(1+\mathrm{i}\eta) - (\omega/\omega_k)^2}, \qquad a_{\mathrm{rx/ry},k}(\omega) = \frac{J''_{\mathrm{rx/ry},k}(1+\mathrm{i}\eta)}{(1+\mathrm{i}\eta) - (\omega/\omega_k)^2} \end{aligned} \tag{8}$$

where n_{m} modes of interest have been considered and α_{st} includes the quasi-static contributions of higher order modes.

3. Effective medium modelling of multi-modal metamaterial panels in real-world scenarios

In this Section, the effective medium modelling framework presented in Section 2 is generalized towards real-world scenarios, to address finite-size

effects, arbitrary boundary conditions, and non-uniform resonator distributions. This is achieved by developing appropriate effective medium models for finite-sized metamaterial panels and coupling them with diffuse STL predictions based on Det-SEA. The features of the Det-SEA approach are first discussed. For the special but important case of simply supported rectangular panels with uniformly distributed resonators, an analytical effective medium model is first developed by exploiting the sinusoidal mode shapes of the bare plate. To consider general boundary conditions and resonator distributions, effective medium plate finite elements are then developed.

3.1. Det-SEA modelling framework for diffuse STL predictions

When considering an indoor setting, i.e. a source room (room 1) and a receiver room (room 2) with an interposed partition panel, the sound fields are commonly taken to be diffuse. The airborne sound insulation is therefore characterized by the diffuse STL. This can be computed through the Det-SEA framework [25], which allows the rigorous coupling of a detailed model of the finite panel, accounting for its boundary conditions, with a diffuse model of the surrounding sound fields. The computed diffuse STL represents the average insulation performance of the panel across a wide range of situations (e.g. across an ensemble of possible source and receiver rooms). The Det-SEA framework has been used to predict the sound insulation of complex partition elements, e.g. composite metamaterial panels [43], double walls [44] and thick or layered wall and floor systems [45, 24].

In the diffuse model, the sound fields in the rooms are decomposed into a direct field and a reverberant field. The direct field is deterministic and describes waves travelling away from the panel, due to its vibration, i.e. the sound fields that occur if the rooms behave as acoustic half-spaces. The reverberant field is stochastic and represents reflected and scattered waves travelling back to the panel. By making use of diffuse field reciprocity [46], it is possible to express the ensemble-average reverberant field response of the rooms as a function of the direct field response. The diffuse field sound transmission coefficient is therefore evaluated by considering the interaction between the panel and the direct field response of the rooms. This interaction is expressed through the direct field dynamic stiffness matrices $\boldsymbol{D}_{\mathrm{d1}}$ and $\boldsymbol{D}_{\mathrm{d2}}$, for room 1 and room 2 respectively, which can be computed numerically via approximation of the Rayleigh integral, e.g. using a wavelet discretization of the baffled interface [47].

The direct field dynamic stiffness matrices are summed to the in-vacuo dynamic stiffness matrix of the panel $\boldsymbol{D}$ to obtain the total dynamic stiffness matrix $\boldsymbol{D}_{\mathrm{t}}$ of the coupled system:

$$\boldsymbol{D}_{\mathrm{t}} := \boldsymbol{D} + \boldsymbol{D}_{\mathrm{d1}} + \boldsymbol{D}_{\mathrm{d2}} \tag{9}$$

The diffuse field sound transmission coefficient is finally evaluated as [25]:

$$\tau_{\mathrm{d}} = \frac{16\pi c^2}{L_{\mathrm{px}} L_{\mathrm{py}} \omega^2} \sum_{rs} \mathrm{Im}(\boldsymbol{D}_{\mathrm{d2}})_{rs} (\boldsymbol{D}_{\mathrm{t}}^{-1} \mathrm{Im}(\boldsymbol{D}_{\mathrm{d1}}) \boldsymbol{D}_{\mathrm{t}}^{-H})_{rs} \tag{10}$$

where L_{px}, L_{py} are the planar dimensions of the panel. Since D_{d1}, D_{d2} and D_{t} are usually full matrices, solving Eq. (10) can be computationally inefficient. For this reason, the problem is usually projected onto a reduced set of modal basis functions, e.g. by considering the structural eigenmodes below twice the maximum frequency of the analysis.

The dynamic stiffness matrix $\boldsymbol{D}$ of the panel can be obtained through a detailed finite element (detailed FEM) discretization. However, when considering metamaterial panels with complex resonator layouts, the size of the FE model and the computational cost of the associated calculations increase significantly. In what follows, we develop effective medium models for finite metamaterial panels that reduce the model size and increase computational efficiency.

3.2. Analytical effective medium modelling of simply supported rectangular metamaterial panels

For simply supported rectangular metamaterial panels, an analytical effective medium model is developed to obtain the dynamic stiffness matrix. The dynamic stiffness matrix is expressed with respect to the modal coordinates of the bare orthotropic panel without attached resonators, i.e. with respect to the following sinusoidal basis functions:

$$\begin{aligned} \phi_j(x,y) &= \frac{2}{\sqrt{\rho h}} \sin(k_{\mathrm{x},j} x) \sin(k_{\mathrm{y},j} y) \\ k_{\mathrm{x},j} &= \frac{n_{\mathrm{x},j}\pi}{L_{\mathrm{px}}}, \quad k_{\mathrm{y},j} = \frac{n_{\mathrm{y},j}\pi}{L_{\mathrm{py}}} \end{aligned} \tag{11}$$

The natural frequencies associated with each mode shape $\phi_j(x,y)$ of the bare panel are:

$$\omega_j = \sqrt{\frac{1}{\rho h^2} \left(D_{\mathrm{x}} k_{\mathrm{x},j}^4 + 2H k_{\mathrm{x},j}^2 k_{\mathrm{y},j}^2 + D_{\mathrm{y}} k_{\mathrm{y},j}^4 \right)} \tag{12}$$

The dynamic stiffness matrix of the metamaterial panel is obtained from the effective diagonal modal mass matrix $\boldsymbol{M}$ and the diagonal modal stiffness matrix $\boldsymbol{K}$:

$$\begin{aligned}\boldsymbol{D} &= -\omega^2\boldsymbol{M} + \boldsymbol{K}(1+\mathrm{i}\eta_0)\\ \boldsymbol{M} &= \mathrm{diag}\left(\frac{\rho_{\mathrm{eff,1}}}{\rho}, \frac{\rho_{\mathrm{eff,2}}}{\rho}, ..., \frac{\rho_{\mathrm{eff,n}}}{\rho}\right)\\ \boldsymbol{K} &= \mathrm{diag}\left(\omega_1^2, \omega_2^2, ..., \omega_{\mathrm{n}}^2\right)\end{aligned} \tag{13}$$

In Eq. (13), the modal mass contributions are scaled through the modal effective mass densities, which depend on the frequency of analysis and on the modal wavenumbers $k_{\mathrm{x},j}$ and $k_{\mathrm{y},j}$:

$$\frac{\rho_{\mathrm{eff},j}}{\rho} = \alpha_{\mathrm{st}} + \frac{1}{\rho h}\sum_{k=1}^{n_{\mathrm{m}}}\left(a_{\mathrm{z},k}(\omega) + a_{\mathrm{rx},k}(\omega)k_{\mathrm{y},j}^2 + a_{\mathrm{ry},k}(\omega)k_{\mathrm{x},j}^2\right) \tag{14}$$

3.3. Effective medium finite elements for general boundary conditions and non-uniform resonator distributions

For metamaterial panels with general boundary conditions and non-uniform resonator distributions, the mode shapes of the bare plate do not have an analytical closed-form expression. Since they are not simple sine functions with a straightforwardly defined wavenumber, it is not possible to directly define the modal mass contributions as in Section 3.2. To treat these general cases, we develop effective medium plate finite elements, which are based on the homogenized effective properties.

In the presence of multi-modal resonators, the harmonic equations of motion of the metamaterial panel become:

$$\begin{aligned}&\left(D_{\mathrm{x}}\frac{\partial^4\overline{w}}{\partial x^4} + 2H\frac{\partial^4\overline{w}}{\partial x^2\partial y^2} + D_{\mathrm{y}}\frac{\partial^4\overline{w}}{\partial y^4}\right)(1+\mathrm{i}\eta_0)\\ &\qquad\underbrace{-\omega^2\left(\overline{a}_{\mathrm{z}}(\omega)\overline{w} - \overline{a}_{\mathrm{rx}}(\omega)\frac{\partial^2\overline{w}}{\partial y^2} - \overline{a}_{\mathrm{ry}}(\omega)\frac{\partial^2\overline{w}}{\partial x^2}\right)}_{f''_{\mathrm{in}}} = p\end{aligned} \tag{15}$$

where:

$$\overline{a}_{\mathrm{z}}(\omega) = \rho\alpha_{\mathrm{st}} + \sum_{k=1}^{n_{\mathrm{m}}} a_{\mathrm{z},k}(\omega), \qquad \overline{a}_{\mathrm{rx/ry}}(\omega) = \sum_{k=1}^{n_{\mathrm{m}}} a_{\mathrm{rx/ry},k}(\omega) \tag{16}$$

The second addend at the left-hand side of Eq. (15) represents the harmonic inertial forces per unit of area f''_{in}.

The equations of motion in Eq. (15) can be written in weak form by considering a virtual displacement field $\overline{v}(x, y)$ on the metamaterial panel domain Ω. For the inertial terms, this leads to:

$$\begin{aligned} F_{\text{in}} &= \int_{\Omega} \overline{v}\, f''_{\text{in}} \mathrm{d}\Omega \\ &= -\omega^2 \left(\int_{\Omega} \overline{v}\, \overline{a}_{\text{z}}(\omega) \overline{w} \mathrm{d}\Omega - \int_{\Omega} \overline{v}\, \overline{a}_{\text{rx}}(\omega) \frac{\partial^2 \overline{w}}{\partial y^2} \mathrm{d}\Omega - \int_{\Omega} \overline{v}\, \overline{a}_{\text{ry}}(\omega) \frac{\partial^2 \overline{w}}{\partial x^2} \mathrm{d}\Omega \right) \end{aligned} \tag{17}$$

Integrating by parts the last two terms leads to:

$$\begin{aligned} -\int_{\Omega} \overline{v}\, \overline{a}_{\text{rx}}(\omega) \frac{\partial^2 \overline{w}}{\partial y^2} \mathrm{d}\Omega &= -\cancel{\int_{\Gamma} \overline{v}\, \overline{a}_{\text{rx}}(\omega) \frac{\partial \overline{w}}{\partial y} \mathrm{d}\Gamma} + \int_{\Omega} \frac{\partial \overline{v}}{\partial y} \overline{a}_{\text{rx}}(\omega) \frac{\partial \overline{w}}{\partial y} \mathrm{d}\Omega \\ -\int_{\Omega} \overline{v}\, \overline{a}_{\text{ry}}(\omega) \frac{\partial^2 \overline{w}}{\partial x^2} \mathrm{d}\Omega &= -\cancel{\int_{\Gamma} \overline{v}\, \overline{a}_{\text{ry}}(\omega) \frac{\partial \overline{w}}{\partial x} \mathrm{d}\Gamma} + \int_{\Omega} \frac{\partial \overline{v}}{\partial x} \overline{a}_{\text{ry}}(\omega) \frac{\partial \overline{w}}{\partial x} \mathrm{d}\Omega \end{aligned} \tag{18}$$

where we have considered that the virtual displacement field is null at the boundary Γ of the metamaterial panel domain, complying with simply supported or clamped boundary conditions.

Next, the FE discretization is introduced by approximating the displacement field as $\overline{w}(x, y) \approx \boldsymbol{N}(x, y)\boldsymbol{w}_{\mathbf{N}}$, where $\boldsymbol{N}(x, y)$ is the vector of globally defined shape functions and $\boldsymbol{w}_{\mathbf{N}}$ is the vector of nodal degrees of freedom. A standard Galerkin procedure is followed, where the same discretization is considered for the virtual displacement field, i.e. $\overline{v}(x, y) \approx \boldsymbol{N}(x, y)\boldsymbol{v}_{\mathbf{N}}$. These steps lead to:

$$\begin{aligned} F_{\text{in}} = -\omega^2 {\boldsymbol{v}_{\mathbf{N}}}^{\mathrm{T}} \Bigg(&\int_{\Omega} \overline{a}_{\text{z}}(\omega) \boldsymbol{N}^{\mathrm{T}} \boldsymbol{N} \mathrm{d}\Omega + \int_{\Omega} \overline{a}_{\text{rx}}(\omega) \left(\frac{\partial \boldsymbol{N}}{\partial y} \right)^{\mathrm{T}} \frac{\partial \boldsymbol{N}}{\partial y} \mathrm{d}\Omega \\ &+ \int_{\Omega} \overline{a}_{\text{ry}}(\omega) \left(\frac{\partial \boldsymbol{N}}{\partial x} \right)^{\mathrm{T}} \frac{\partial \boldsymbol{N}}{\partial x} \mathrm{d}\Omega \Bigg) \boldsymbol{w}_{\mathbf{N}} \end{aligned} \tag{19}$$

Eq. (19) yields the frequency-dependent mass matrix of the metamaterial panel, which is the sum of different terms associated with the translational and rotational contributions of the resonators:

$$\boldsymbol{M}(\omega) = \boldsymbol{M}_{\mathbf{z}}(\omega) + \boldsymbol{M}_{\mathbf{rx}}(\omega) + \boldsymbol{M}_{\mathbf{ry}}(\omega) \tag{20}$$

with:

$$\begin{aligned}
\boldsymbol{M}_{\mathbf{z}}(\omega) &= \int_{\Omega} \overline{a}_{\mathrm{z}}(\omega) \boldsymbol{N}^{\mathrm{T}} \boldsymbol{N} \mathrm{d}\Omega \\
\boldsymbol{M}_{\mathbf{rx}}(\omega) &= \int_{\Omega} \overline{a}_{\mathrm{rx}}(\omega) \left(\frac{\partial \boldsymbol{N}}{\partial y} \right)^{\mathrm{T}} \frac{\partial \boldsymbol{N}}{\partial y} \mathrm{d}\Omega \\
\boldsymbol{M}_{\mathbf{ry}}(\omega) &= \int_{\Omega} \overline{a}_{\mathrm{ry}}(\omega) \left(\frac{\partial \boldsymbol{N}}{\partial x} \right)^{\mathrm{T}} \frac{\partial \boldsymbol{N}}{\partial x} \mathrm{d}\Omega
\end{aligned} \tag{21}$$

Eq. (21) shows that translational resonator contributions are included in the matrix $\boldsymbol{M}_{\mathbf{z}}(\omega)$, which mirrors common FEM mass matrices while including frequency-dependent mass properties through $\overline{a}_{\mathrm{z}}(\omega)$. On the contrary, rotational resonator contributions are included in the frequency-dependent mass matrices $\boldsymbol{M}_{\mathbf{rx}}(\omega)$ and $\boldsymbol{M}_{\mathbf{ry}}(\omega)$, which have a different form than common FEM matrices and include the spatial derivatives of the shape functions.

The dynamic stiffness matrix of the metamaterial panel discretized by the effective medium finite elements is finally written as:

$$\boldsymbol{D}(\omega) = -\omega^2 \boldsymbol{M}(\omega) + \boldsymbol{K}(1 + \mathrm{i}\eta_0) \tag{22}$$

where $\boldsymbol{K}$ is the same stiffness matrix as in standard FEM.

The developed formulation can account for metamaterial panels with general shape and for an arbitrary distribution of simply supported and clamped boundary conditions at the edges. Also, arbitrary distributions of the resonators can be modelled by considering terms $\overline{a}_{\mathrm{z}}(\omega)$, $\overline{a}_{\mathrm{rx/ry}}(\omega)$ that vary within the metamaterial panel domain. We note that in Eq. (18) the spatial derivatives of the terms $\overline{a}_{\mathrm{rx/ry}}$ have been neglected, which is valid for slowly varying resonator distributions within each finite element. If these derivatives cannot be neglected, e.g. for graded metamaterials, they should be accounted for in the integration by parts.

4. Results and discussion

In this Section, the effective medium approaches developed in Section 3 are used to study the vibroacoustic properties of two showcase multi-modal metamaterial panels in real-world scenarios, when varying the panel dimensions, the applied boundary conditions, and the treatment area.

The same showcase multi-modal metamaterial panels as in [20] are considered (Figures 3a and 3b), which introduce both a 20% additional mass

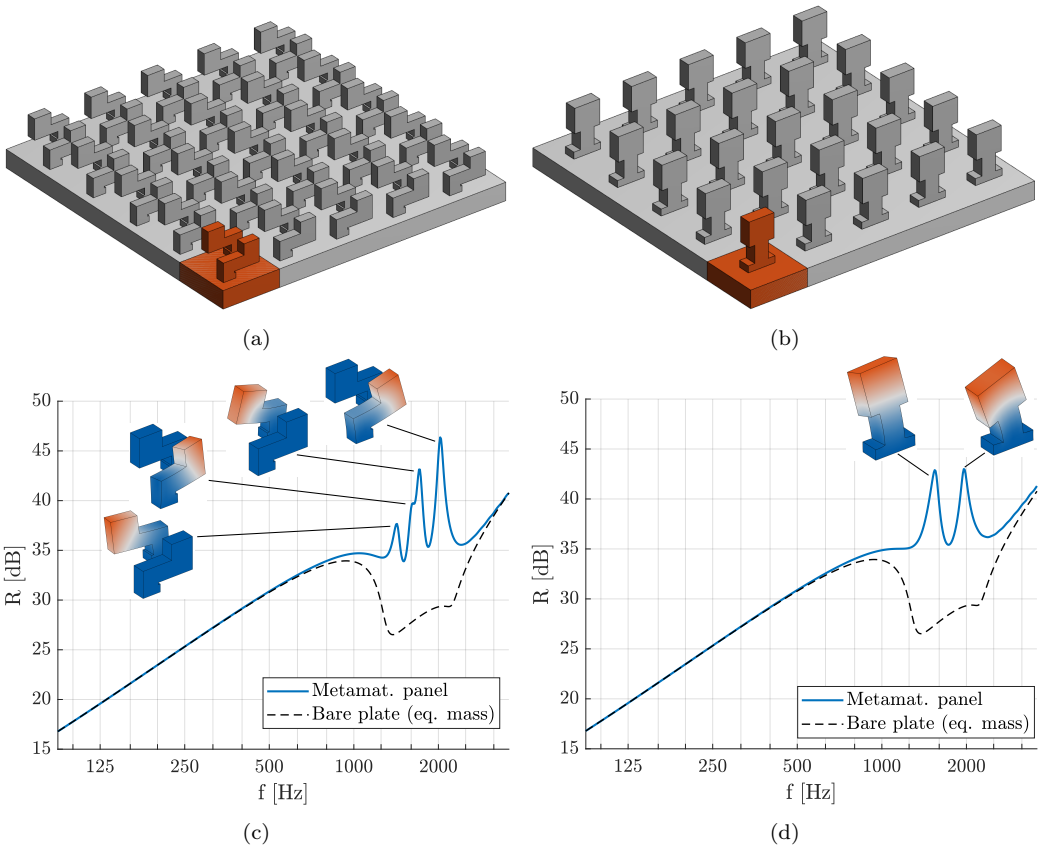


Figure 3: (a,b) considered multi-modal metamaterial panels and (c,d) related STL predictions for infinite size. The metamaterial panels include (a,c) double translational and (b,d) double rotational resonators.

with respect to the host plate (the mass ratio is $\gamma = 0.2$) and include resonators in PMMA ($E = 4850$ MPa, $\nu = 0.31$, $\rho = 1200$ kg/m^3, $\eta = 0.05$). The first "double translational" resonator (Figure 3a) consists of two horizontal cantilever beams with attached end-point masses and exhibits four modes of interest, related to the vertical translation and the rotation of the two masses. The second "double rotational" resonator (Figure 3b) consists of a mass attached to a vertical beam and exhibits the two modes of interest, related to rotations of the mass around the x and y axes.

The STL of the two showcase metamaterial panels for infinite panel dimensions is shown in Figures 3c and 3d. In both cases, the resonator modes have been distributed to suppress the broad STL dip of the bare host plate by introducing multiple STL peaks. Broadband STL improvements around 5-10 dB are obtained in the whole coincidence dip range, with respect to a bare plate with equivalent mass.

Figure 4 shows the STL of simply supported rectangular metamaterial panels for the double translational and the double rotational resonator layouts. Figure 5 shows the STL of double rotational metamaterial panels when considering clamped boundary conditions on the 4 edges, as well as partial metamaterial treatment, i.e. resonators distributed only on one half of a simply-supported panel. In the presented examples, the Rayleigh integral for the computation of the direct field dynamic stiffness matrices is approximated on a 0.02 m $\times$ 0.02 m grid, which at the maximum frequency of the analysis corresponds to 6 discretization points per minimum wavelength propagating in the bare plate. The same 0.02 m $\times$ 0.02 m discretization has been used in effective medium FEM models, in which each element includes 4 nodes and bilinear shape functions.

The effect of the panel size on the STL is studied by comparing 0.6 m $\times$ 0.45 m and 1.5 m $\times$ 1.25 m panels, and is highlighted in Figures 4e and 4f for the simply supported case. It is shown that reducing the dimensions mainly influences the modal behaviour of the panel, as more prominent STL dips due to panel resonances are introduced at low frequencies. Similarly, also the effect of changing the boundary conditions is mainly on the modal behaviour of the panel. The STL dips due to panel resonances shift to higher frequencies when passing from simply-supported (Figures 4b and 4d) to fully clamped (Figures 5a and 5c) panels, following the increased stiffness around the boundary regions. The effect of panel dimensions and boundary conditions is, instead, minimal on the entity of the resonance STL peaks introduced by the metamaterial treatment. When changing these parameters in fact, the

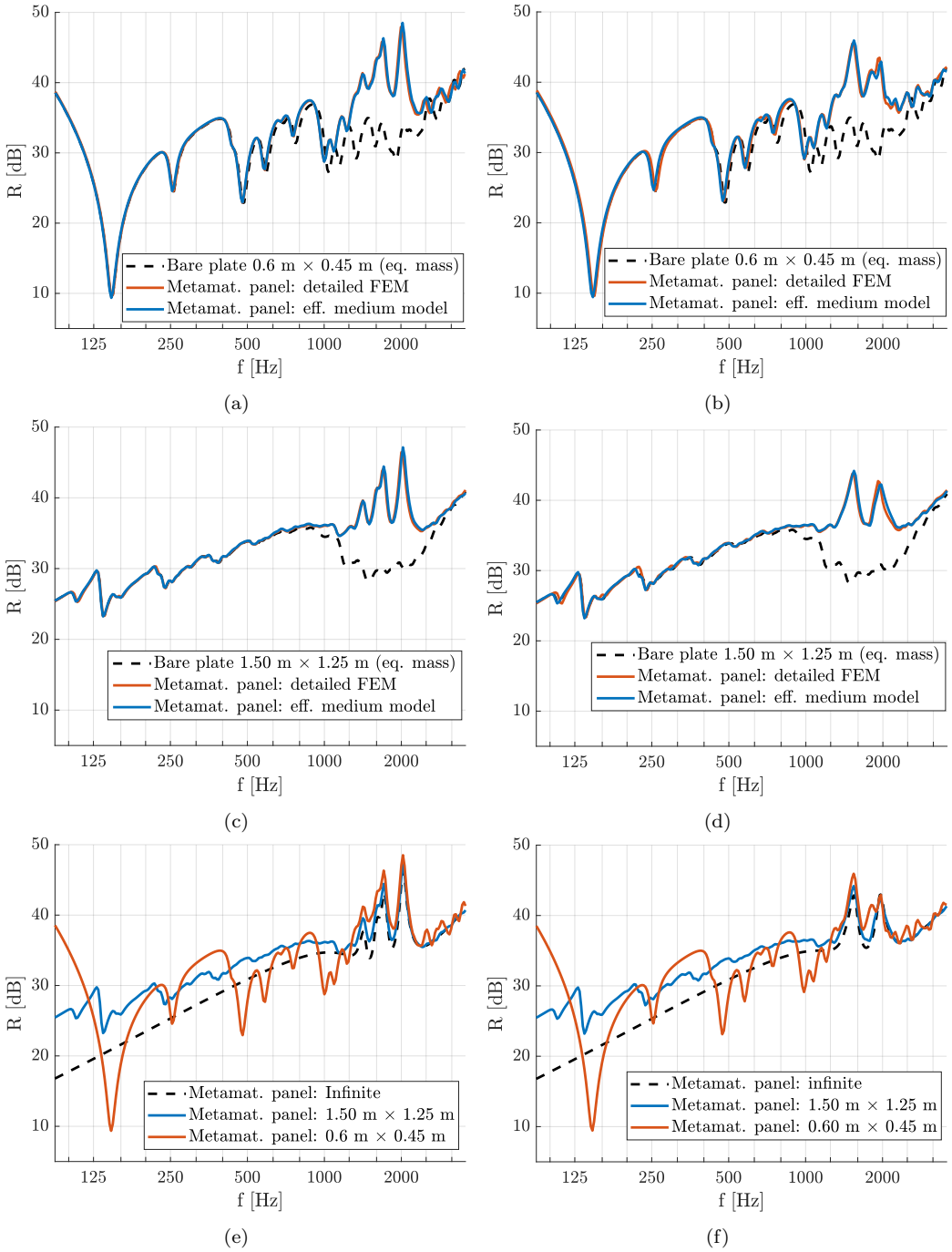


Figure 4: Det-SEA STL predictions for simply supported rectangular metamaterial panels: validation of the effective medium model for double translational (a,c,e) and double rotational (b,d,f) resonators. Metamaterial panel size: (a,b) 0.6 m × 0.45 m, (c,d) 1.5 m × 1.25 m, (e,f) varying.

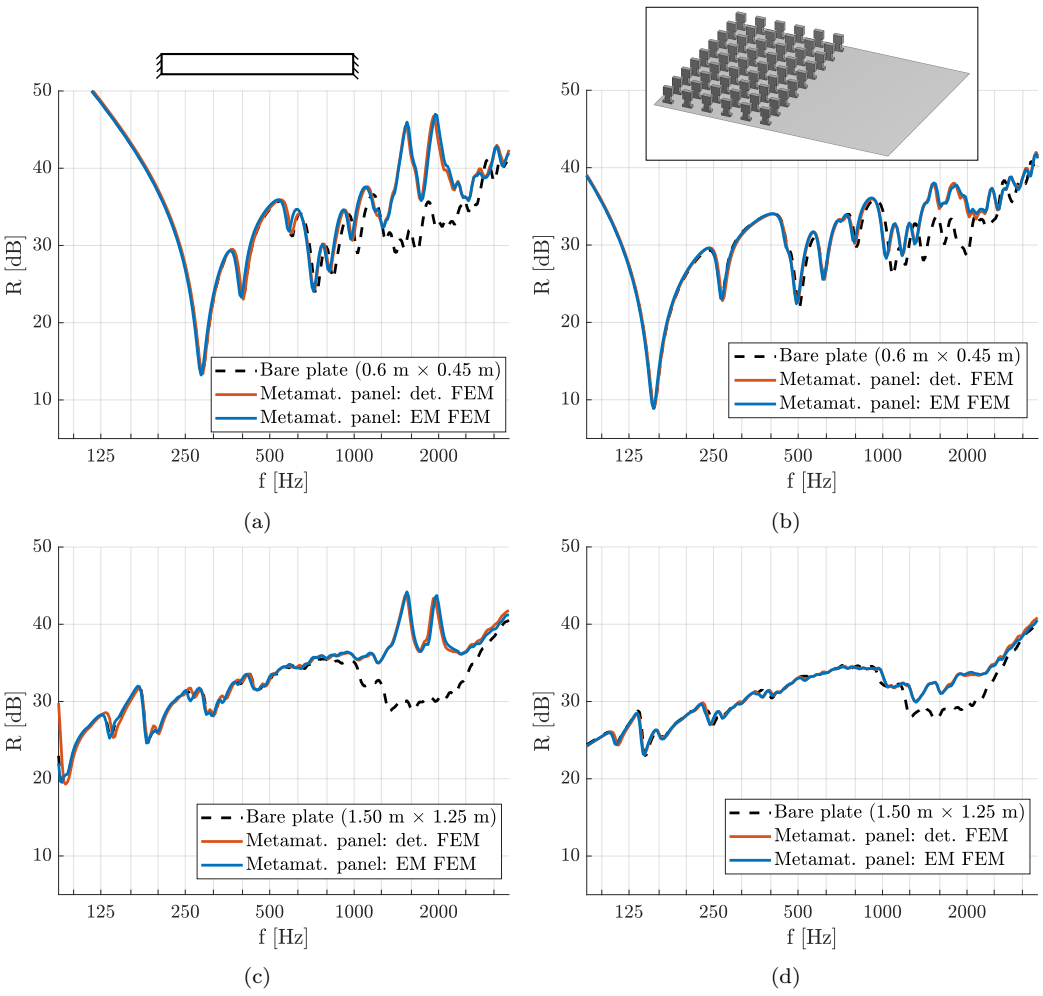


Figure 5: Validation of the proposed effective medium FEM formulation (EM FEM) through Det-SEA STL predictions for (a,c) clamped and (b,d) partially treated metamaterial panels. Metamaterial panel size: (a,b) 0.6 m × 0.45 m, (c,d) 1.5 m × 1.25 m.

Table 1: Comparison of computational costs between effective medium modelling and detailed FEM for simply supported rectangular metamaterial panels.

Metamaterial panel		**Double transl. res.**		**Double rot. res.**	
Dimensions [m^2]		**0.6 x 0.45**	**1.5 x 1.25**	**0.6 x 0.45**	**1.5 x 1.25**
Detailed FEM + Craig-Bampton	n_{DOFs}	19 736	129 680	18 581	121 955
	n_{modes}	852	5993	421	3008
	t_{modes}	2 min 22 s	3 h 11 min	59.4 s	1 h 10 min
	t_{Dd}	9.0 s	12 min 55 s	5.7 s	4 min 51 s
	t_{TL}	20.4 s	8 min 6 s	4.4 s	1 min 35 s
	$\boldsymbol{t_{\text{tot}}}$	**2 min 51 s**	**3 h 32 min**	**1 min 10 s**	**1 h 17 min**
Effective medium model	n_{modes}	100	529	100	529
	t_{Dd}	3.5 s	2 min 1 s	3.5 s	2 min 1 s
	t_{TL}	0.9 s	5.2 s	0.9 s	5.2 s
	$\boldsymbol{t_{\text{tot}}}$	**4.4 s**	**2 min 6 s**	**4.4 s**	**2 min 6 s**

average STL improvements with respect to the bare host plate keep around 5-10 dB in the coincidence dip. The amplitude of the STL peaks depends mostly on the amount of distributed resonators: when halving the amount of resonator through partial metamaterial treatment (Figures 5b and 5d), the average STL improvements in the coincidence dip decrease to 3-5 dB.

The use of the proposed effective medium models in Det-SEA STL predictions is validated against the use of detailed FEM models. The detailed FEM models are built by coupling together 12 $\times$ 9 unit cell models for 0.6 m $\times$ 0.45 m metamaterial panels and 30 $\times$ 25 unit cell models for 1.5 m $\times$ 1.25 m panels. Each unit cell model considers a discretization of the host plate by linear Kirchhoff shell finite elements and a discretization of the resonators by linear hexahedral finite elements [20]. After Craig-Bampton reduction with 12 internal modes, the unit cell models of the metamaterial panels include 332 degrees of freedom (DOFs) and 312 DOFs for the double translational and the double rotational resonator layouts respectively.

For all the considered cases, the effective medium model preserves the model accuracy of detailed FEM within the whole frequency range of interest. A comparison of computational costs between the two approaches is reported in Tables 1 and 2. The focus is on the total number of DOFs n_{DOFs} and the total CPU time t_{tot}, when a Matlab implementation on an Intel(R) Core(TM) i9-10900X CPU (3.70 GHz) is considered.

The model size reduction between detailed FEM and effective medium modelling is by 2 orders of magnitude for simply supported metamaterial

Table 2: Comparison of computational costs between effective medium FEM and detailed FEM for fully clamped and partially treated rectangular metamaterial panels.

Metamaterial panel		**Clamped**		**Partially treated**	
Dimensions [m^2]		**0.6 x 0.45**	**1.5 x 1.25**	**0.6 x 0.45**	**1.5 x 1.25**
Detailed FEM + Craig-Bampton	n_{DOFs}	18 581	121 955	18 581	121 955
	n_{modes}	414	2986	255	1836
	t_{modes}	56.4 s	1 h 8 min	35.7 s	36 min 19 s
	t_{Dd}	5.0 s	4 min 46 s	3.9 s	3 min 0 s
	t_{TL}	4.2 s	1 min 33 s	1.0 s	2 min 37 s
	$\boldsymbol{t_{\text{tot}}}$	**1 min 6 s**	**1 h 15 min**	**40.6 s**	**41 min 56 s**
Effective medium FEM	n_{DOFs}	2475	15987	2475	15987
	n_{modes}	64	522	72	541
	t_{modes}	0.2 s	9.7 s	0.2 s	10.2 s
	t_{Dd}	2.3 s	1 min 37 s	2.3 s	1 min 40 s
	t_{TL}	0.5 s	10.4 s	0.2 s	10.6 s
	$\boldsymbol{t_{\text{tot}}}$	**3.0 s**	**1 min 57 s**	**2.7 s**	**2 min 1 s**

panels and by one order of magnitude for the effective medium finite element approach. It is shown that also the required amount n_{modes} of modes to be computed for the reduction of Eq. (10) is decreased. Within effective medium modelling, the local modes of the attached resonators are directly considered by modulating the effective inertia according through the terms $\overline{a}_{\text{z}}(\omega)$, $\overline{a}_{\text{rx}}(\omega)$, $\overline{a}_{\text{ry}}(\omega)$, therefore the sole computation of the bare structure modes is needed. When using FEM instead, the model includes the detailed coupling of the host structure with the attached resonators, and a higher amount of modes need to be computed to include both global panel modes and local resonances.

The reduction in model size and amount of required modes offered by the effective medium model is followed by a significant reduction in computational costs. The reported total CPU time t_{tot} accounts for the times to compute the required modes (t_{modes}), the direct field dynamic stiffness matrices (t_{Dd}), and the transmission loss (t_{TL}). Results show that the CPU time of effective medium model predictions is one to two orders of magnitude smaller than detailed FEM.

5. Conclusions

In this work, a generalized effective medium modelling framework has been developed to study the behaviour of multi-modal metamaterial panels

in real-world scenarios, which handles finite-size effects, arbitrary boundary conditions, and non-uniform resonator distributions.

A methodology to efficiently compute the diffuse STL of real-world metamaterial panels has been established. This is based on the deterministic-statistical energy analysis (Det-SEA) approach, in which an effective medium model of the finite panel is coupled with a diffuse description of the surrounding sound fields. For the special but important the case of simply supported rectangular metamaterial panels with uniformly distributed resonators, an analytical effective medium model has been derived by exploiting the sinusoidal mode shapes of the bare plate. To include more general boundary conditions and resonator distributions, effective medium plate finite elements have been formulated.

The proposed effective medium modelling approach has been employed in the study of two showcase metamaterial panels, which successfully achieve the suppression of the broadband sound insulation dip due to coincidence in orthotropic host plates. The analysis of finite-size effects has shown that reducing the dimensions of the panel induces more prominent STL dips at low frequencies, which are due to the modal behaviour of the panel and depend on the applied boundary conditions. The panel dimensions and the boundary conditions have, instead, a minor influence on the entity of the resonance peaks introduced by the metamaterial treatment, which depends mostly on the amount of distributed resonators.

Furthermore, the accuracy of the presented effective medium methodologies has been validated against detailed finite element modelling. It has been demonstrated that the proposed approaches allow for a significant reduction in computational costs while preserving accuracy.

The presented study significantly advances the understanding and modeling capabilities of multi-modal metamaterial panels, holding promising implications for their design optimization in functional applications.

Acknowledgments

This research was funded by the European Research Council (ERC) Executive Agency, through the ERC Starting Grant 714591 VirBAcous provided to Edwin Reynders under the Horizon 2020 framework program, and by Research Foundation - Flanders (FWO), through the postdoctoral fellowship 12A3Q24N provided to Daniele Giannini. The financial supports from ERC and FWO are gratefully acknowledged.

References

[1] Z. Liu, X. Zhang, Y. Mao, Y. Y. Zhu, Z. Yang, C. Chan, P. Sheng, Locally resonant sonic materials, Science 289 (5485) (2000) 1734–1736.

[2] L. Fok, M. Ambati, X. Zhang, Acoustic metamaterials, MRS Bulletin 33 (10) (2008) 931–934.

[3] G. Ma, P. Sheng, Acoustic metamaterials: From local resonances to broad horizons, Science Advances 2 (2) (2016) e1501595.

[4] Y. Xiao, J. Wen, X. Wen, Sound transmission loss of metamaterial-based thin plates with multiple subwavelength arrays of attached resonators, Journal of Sound and Vibration 331 (25) (2012) 5408–5423.

[5] A. Hall, E. Calius, G. Dodd, E. Wester, K. Chan, Development of locally resonant structures for sonic barriers, Building Acoustics 21 (3) (2014) 199–220.

[6] B. Assouar, M. Oudich, X. Zhou, Sound insulation and energy harvesting based on acoustic metamaterial plate, in: T. Kundu (Ed.), Health Monitoring of Structural and Biological Systems 2015, Vol. 9438 of Society of Photo-Optical Instrumentation Engineers (SPIE) Conference Series, 2015, p. 94380U.

[7] C. Claeys, E. Deckers, B. Pluymers, W. Desmet, A lightweight vibro-acoustic metamaterial demonstrator: Numerical and experimental investigation, Mechanical Systems and Signal Processing 70-71 (2016) 853–880.

[8] C. Goffaux, J. Sánchez-Dehesa, A. L. Yeyati, P. Lambin, A. Khelif, J. Vasseur, B. Djafari-Rouhani, Evidence of fano-like interference phenomena in locally resonant materials, Physical Review Letters 88 (2002) 225502.

[9] F. Lemoult, N. Kaina, M. Fink, G. Lerosey, Wave propagation control at the deep subwavelength scale in metamaterials, Nature Physics 9 (2013) 55–60.

[10] C. Claeys, K. Vergote, P. Sas, W. Desmet, On the potential of tuned resonators to obtain low-frequency vibrational stop bands in periodic panels, Journal of Sound and Vibration 332 (6) (2013) 1418–1436.

[11] L. Van Belle, C. Claeys, E. Deckers, W. Desmet, The impact of damping on the sound transmission loss of locally resonant metamaterial plates, Journal of Sound and Vibration 461 (2019) 114909.

[12] G. L. Huang, C. T. Sun, Band Gaps in a Multiresonator Acoustic Metamaterial, Journal of Vibration and Acoustics 132 (3), 031003 (04 2010).

[13] Y. Chen, M. Barnhart, J. Chen, G. Hu, C. Sun, G. Huang, Dissipative elastic metamaterials for broadband wave mitigation at subwavelength scale, Composite Structures 136 (2016) 358–371.

[14] D. Roca, J. Cante, O. Lloberas-Valls, T. Pàmies, J. Oliver, Multiresonant layered acoustic metamaterial (MLAM) solution for broadband low-frequency noise attenuation through double-peak sound transmission loss response, Extreme Mechanics Letters 47 (2021) 101368.

[15] C. Claeys, N. Rocha de Melo Filho, L. Van Belle, E. Deckers, W. Desmet, Design and validation of metamaterials for multiple structural stop bands in waveguides, Extreme Mechanics Letters 12 (2017) 7–22, frontiers in Mechanical Metamaterials.

[16] C. Droz, O. Robin, M. Ichchou, N. Atalla, Improving sound transmission loss at ring frequency of a curved panel using tunable 3d-printed small-scale resonators, The Journal of the Acoustical Society of America 145 (1) (2019) EL72–EL78.

[17] S. Ning, F. Yang, C. Luo, Z. Liu, Z. Zhuang, Low-frequency tunable locally resonant band gaps in acoustic metamaterials through large deformation, Extreme Mechanics Letters 35 (2020) 100623.

[18] V. Romero-García, A. Krynkin, L. Garcia-Raffi, O. Umnova, J. Sánchez-Pérez, Multi-resonant scatterers in sonic crystals: Locally multi-resonant acoustic metamaterial, Journal of Sound and Vibration 332 (1) (2013) 184–198.

[19] H. Meng, D. Chronopoulos, A. Fabro, W. Elmadih, I. Maskery, Rainbow metamaterials for broadband multi-frequency vibration attenuation: Numerical analysis and experimental validation, Journal of Sound and Vibration 465 (2020) 115005.

[20] D. Giannini, M. Schevenels, E. Reynders, Rotational and multimodal local resonators for broadband sound insulation of orthotropic metamaterial plates, Journal of Sound and Vibration 547 (117453) (2023) 1–17.

[21] Y. Yang, B. Mace, M. Kingan, Vibroacoustic analysis of periodic structures using a wave and finite element method, Journal of Sound and Vibration 457 (2019) 333–353.

[22] J. Vazquez Torre, J. Brunskog, V. Cutanda Henriquez, J. Jung, Hybrid analytical-numerical optimization design methodology of acoustic metamaterials for sound insulation, Journal of the Acoustical Society of America 149 (6) (2021) 4398–4409.

[23] Y. Yang, M. Kingan, B. Mace, A wave and finite element method for calculating sound transmission through rectangular panels, Journal of Sound and Vibration 151 (107357) (2021) 1–14.

[24] C. Decraene, G. Lombaert, E. Reynders, Prediction of diffuse sound transmission through finite-sized periodic structures, Journal of Sound and Vibration 528 (2022) 116851.

[25] E. Reynders, C. Van hoorickx, Uncertainty quantification of diffuse sound insulation values, Journal of Sound and Vibration 544 (117404) (2023) 1–15.

[26] R. Lyon, R. DeJong, Theory and application of statistical energy analysis, 2nd Edition, Butterworth-Heinemann, Newton, MA, 1995.

[27] P. Shorter, R. Langley, Vibro-acoustic analysis of complex systems, Journal of Sound and Vibration 288 (2005) 669–699.

[28] E. Reynders, R. Langley, A. Dijckmans, G. Vermeir, A hybrid finite element – statistical energy analysis approach to robust sound transmission modeling, Journal of Sound and Vibration 333 (19) (2014) 4621–4636.

[29] D. Krattiger, M. Hussein, Generalized Bloch mode synthesis for accelerated calculation of elastic band structures, Journal of Computational Physics 357 (2018) 183–205.

[30] P. Li, S. Yao, X. Zhou, G. Huang, G. Hu, Effective medium theory of thin-plate acoustic metamaterials, Journal of the Acoustical Society of America 135 (4) (2014) 1844–1852.

[31] A. Norris, Mechanics of elastic networks, Proceedings of the Royal Society A: Mathematical, Physical and Engineering Sciences 470 (2172) (2014) 20140522.

[32] M. Messner, Optimal lattice-structured materials, Journal of the Mechanics and Physics of Solids 96 (2016) 162–183.

[33] D. R. Smith, S. Schultz, P. Markoš, C. M. Soukoulis, Determination of effective permittivity and permeability of metamaterials from reflection and transmission coefficients, Phys. Rev. B 65 (2002) 195104.

[34] B. Slovick, Z. Yu, S. Krishnamurthy, Generalized effective-medium theory for metamaterials, Phys. Rev. B 89 (2014) 155118.

[35] J. Kim, H. Kim, B. Kim, T. Chang, J. Lim, H. Jin, J. Mun, Y. Choi, K. Chung, J. Shin, S. Fan, S. Kim, Highly tunable refractive index visible-light metasurface from block copolymer self-assembly, Nature Communications 7 (2016) 12911.

[36] X. Jing, Y. Xu, H. Gan, Y. He, Z. Hong, High refractive index metamaterials by using higher order modes resonances of hollow cylindrical nanostructure in visible region, IEEE Access 7 (2019) 144945–144956.

[37] X. Man, Z. Luo, J. Liu, B. Xia, Hilbert fractal acoustic metamaterials with negative mass density and bulk modulus on subwavelength scale, Materials & Design 180 (2019) 107911.

[38] N. Jiménez, J.-P. Groby, V. Romero-García, The Transfer Matrix Method in Acoustics, Springer International Publishing, Cham, 2021, pp. 103–164.

[39] T. Wang, M. Sheng, Z. Guo, Q. Qin, Acoustic characteristics of damped metamaterial plate with parallel attached resonators, Archives of Mechanics 69 (2017) 29–52.

[40] J. Vazquez Torre, J. Brunskog, V. Cutanda Henriquez, An analytical model for broadband sound transmission loss of a finite single leaf wall using a metamaterial, Journal of the Acoustical Society of America 147 (3) (2020) 1697–1708.

[41] L. Van Belle, C. Claeys, E. Deckers, W. Desmet, On the impact of damping on the dispersion curves of a locally resonant metamaterial: Modelling and experimental validation, Journal of Sound and Vibration 409 (2017) 1–23.

[42] F. Fahy, P. Gardonio, Sound and structural vibration: radiation, transmission and response, 2nd Edition, Academic Press, Oxford, UK, 2007.

[43] D. Chronopoulos, I. Antoniadis, T. Ampatzidis, Enhanced acoustic insulation properties of composite metamaterials having embedded negative stiffness inclusions, Extreme Mechanics Letters 12 (2017) 48–54, frontiers in Mechanical Metamaterials.

[44] J. Van den Wyngaert, M. Schevenels, E. Reynders, Predicting the sound insulation of finite double-leaf walls with a flexible frame, Applied Acoustics 141 (2018) 93–105.

[45] C. Decraene, A. Dijckmans, E. Reynders, Fast mean and variance computation of the diffuse sound transmission through finite-sized thick and layered wall and floor systems, Journal of Sound and Vibration 422 (2018) 131–145.

[46] P. Shorter, R. Langley, On the reciprocity relationship between direct field radiation and diffuse reverberant loading, Journal of the Acoustical Society of America 117 (1) (2005) 85–95.

[47] R. Langley, Numerical evaluation of the acoustic radiation from planar structures with general baffle conditions using wavelets, Journal of the Acoustical Society of America 121 (2) (2007) 766–777.